Homology Modeling and Site-Directed Mutagenesis To Identify Selective Inhibitors of Endothelin-Converting Enzyme-2

Khatuna Gagnidze,[†] Sachchidanand,[#,‡] Raphael Rozenfeld,[†] Mihaly Mezei,[#] Ming-Ming Zhou,[#] and Lakshmi A. Devi*[,†]

Department of Pharmacology and Systems Therapeutics and Department of Structural and Chemical Biology, Mount Sinai School of Medicine, One Gustave L. Levy Place, New York, New York 10029

Received December 11, 2007

Endothelin-converting enzyme-2 (ECE-2), a member of M13 family of zinc metallopeptidases, has previously been shown to process a number of neuropeptides including those derived from prodynorphin, proenkephalin, proSAAS, and amyloid precursor protein. ECE-2, unlike ECE-1, exhibits restricted neuroendocrine distribution and acidic pH optimum; it is consistent with a role in the regulation of neuropeptide levels in vivo. Here, we report the generation of a three-dimensional (3D) molecular model of ECE-2 using the crystal structure of neprilysin (EC 3.4.24.11) as a template. On the basis of the predictions made from the molecular model, we mutated and tested two residues, Trp 148 and Tyr 563, in the catalytic site. The mutation of Tyr 563 was found to significantly affect the catalytic activity and inhibitor binding. The molecular model was used to virtually screen a small molecule library of 13 000 compounds. Among the top-scoring compounds three were found to inhibit ECE-2 with high affinity and exhibited specificity for ECE-2 compared to neprilysin. Thus, the model provides a new useful tool to probe the active site of ECE-2 and design additional selective inhibitors of this enzyme.

Introduction

Neuroendocrine peptides are synthesized as large precursor proteins that undergo multiple posttranslational processing steps to generate bioactive peptides. Most of the peptide precursors are cleaved at specific sites that usually contain multiple basic amino acids that are considered to be the "classical" cleavage sites.[1] This cleavage is performed by endoproteases of the subtilisin family of serine proteases, namely, prohormone convertases (PCs[a]).[2] In addition a number of neuropetides have been identified that are generated by processing at "nonclassical" sites that do not contain basic amino acids. These peptides were identified among the bulk-purified peptides of neuroendocrine tissues and also detected in the brains from mice lacking specific processing enzymes such as CPE.[3–6] In addition, an examination of precursor sequences of some endogenous peptides showed that nonclassical cleavage is needed in order to generate the active forms of these peptides.[7–9]

Members of the metalloprotease family have been implicated in the processing of neuroendocrine peptides at nonclassical sites.[10] Among them ECE-2 fits the criteria of a neuropeptide processing enzyme. ECE-2 is a member of the neprilysin family of Zn^{2+} metallopeptidases and shares most of the common features of this family. It is a type II integral membrane protein with a short cytoplasmic tail, transmembrane domain, and a large C-terminal domain that contains the active site. ECE-2 shares 37% overall homology with neprilysin (NEP) and contains consensus sequences (such as HExxH and ExxxD) involved in Zn^{2+} coordination and catalysis, which are highly conserved among NEP family members. Moreover, the ectodomain of ECE-2 includes 10 cysteine residues and multiple glycosylation sites that are also conserved among family members.[9,11] ECE-2 cleaves its substrates at the amino-terminal side of aromatic or aliphatic residues and is inhibited by the generic inhibitor of metalloproteases, phosphoramidon, with a nanomolar potency.[12–14] ECE-2 converts big endothelin-1 to ET-1 by cleaving the Trp-Val site, a property shared by its close homologue, ECE-1.[12,13,15] Both of these enzymes have also been shown to process β-amyloid peptides and modulate their levels in the mouse brain.[16,17] We have recently reported that ECE-2 is able to cleave a number of neuroendocrine peptide precursors in vitro. The analysis of the cleavage sites revealed that ECE-2 displays endopeptidase-like or peptidyldicarboxypeptidase-like activity and prefers cleaving at sites containing an aromatic or aliphatic residue with a large branched side chain at the P1′ site.[18] It is likely that ECE-2 is involved in the generation of neuropeptides by processing at these "nonclassical" sites.

The physiological functions of ECE-2 or other members of the neprilysin family are not well defined. The structural similarities among NEP family members and the similarities in substrate specificity as well as the overlapping tissue distribution make it difficult to define a distinct role for ECE-2 in neuropeptide processing. A better understanding of the structural architecture of the active site of ECE-2 and its homologues is likely to lead to the delineation of differences in substrate specificity and help us uncover the physiological functions for each of these metalloproteases.

Until recently, the information about the organization of the active site and the residues involved in zinc binding and catalysis of NEP family of enzymes was obtained from multiple mutagenesis studies.[19–26] Early studies examining the catalytic mechanisms of these enzymes used models based on the crystal structure of thermolysin (TLN), a bacterial homologue of NEP.[27,28] The availability of a high resolution crystal structure of NEP complexed with phosphoramidon[11] has allowed the

* To whom correspondence should be addressed. Phone: (212) 241-8345. Fax: (212) 996-7214. E-mail: lakshmi.devi@mssm.edu.

[†] Department of Pharmacology and Systems Therapeutics.

[#] Department of Structural and Chemical Biology.

[‡] Present address: Institute of Life Sciences, University of Hyderabad Campus, Gachibowli, Hyderabad (AP), India, PIN 500046.

[a] Abbreviations: ECE-2, endothelin-converting enzyme; ET, endothelin; NEP, neprilysin; PC, prohormone convertase; CPE, carboxypeptidase; PAM, peptidylglycine α-amidating monooxygenase; TLN, thermolysin; PDB, Protein Data Bank; McaBk2, (7-methoxycoumarin-4-yl)acetyl-RPPGF-SAFL-(2,4-dinitrophenyl); wt, wild type; rmsd, root-mean-squared deviation.

10.1021/jm7015478 CCC: $40.75
Published on Web 05/29/2008

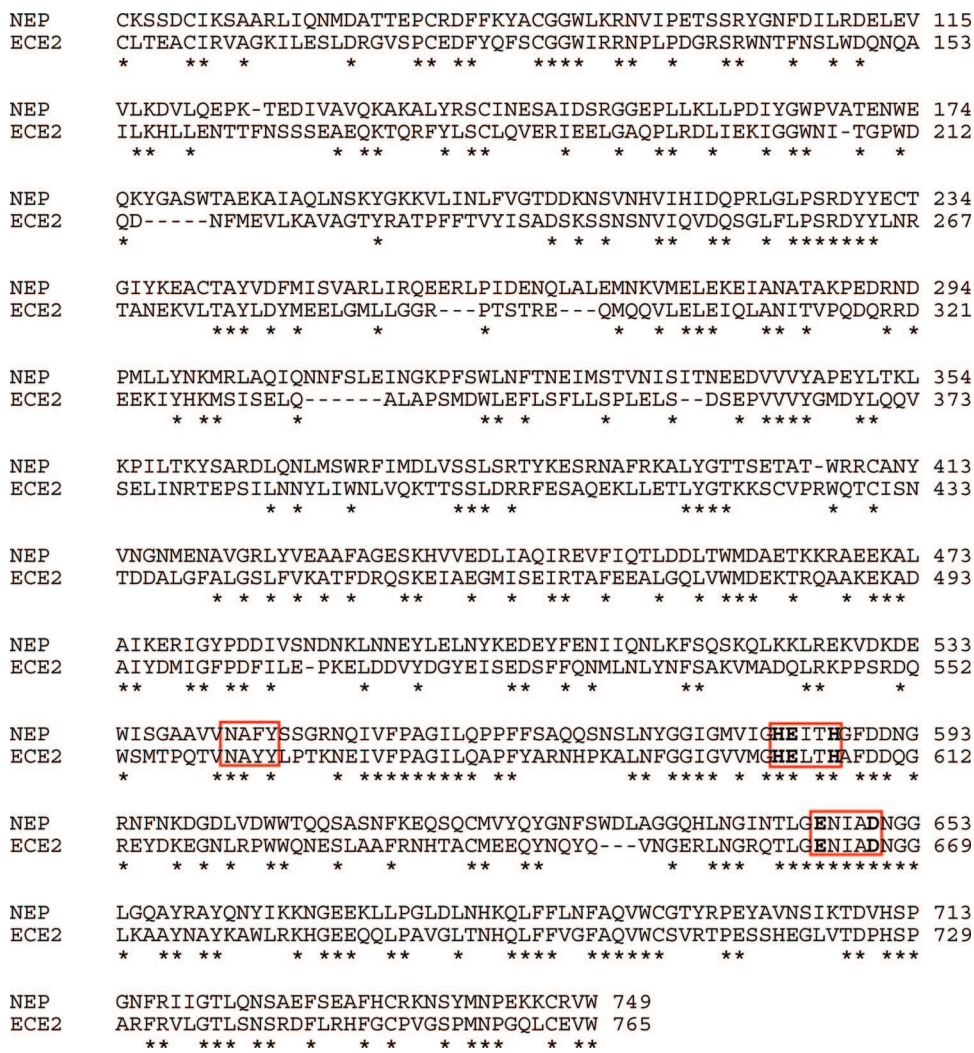

Figure 1. Alignment of human NEP sequence with the sequence of human ECE-2. Alignment was done using ClustalW multiple sequence alignment program. Three regions that are highly conserved and represent consensus sequences are boxed, and the residues participating in zinc binding and coordination as well as in catalysis are shown in bold. The numbers on the right indicate amino acid numbering, and the asterisks indicate conserved residues.

generation of more reliable 3D molecular models for related enzymes. In this study we describe the generation of the homology model of ECE-2. Studies to test the predictions based on the model revealed that Tyr 563, a nonconserved residue of the consensus motif ^{561}NAYY^{564}, plays a role in the catalytic activity and inhibitor binding. We also describe studies identifying ECE-2 selective inhibitors by virtually docking a library of 13 000 small druglike molecules on to the 3D model of ECE-2; this led to the selection of a subset of the compounds that were further screened biochemically. Here, we report the identification of three compounds that inhibit ECE-2 enzyme activity with micromolar potency and display an order of magnitude higher affinity toward ECE-2 compared to NEP.

Results

Modeling of ECE-2. A comparison of the amino acid sequences between neprilysin and ECE-2 reveals a high degree of homology (37%), which suggests that they share a common origin and could share a common fold. On the basis of sequence alignment (Figure 1), it is also clear that the residues around the Zn^{2+} and phosphoramidon binding sites are well conserved between ECE-2 and NEP; thus, it is likely that the homology modeling of ECE-2 using neprilysin structure could be very useful in identifying critical residues involved in substrate/inhibitor binding. We built a 3D molecular model of ECE-2 using the coordinates from the reported crystal structure of NEP (PDB code 1DMT)[11] and checked the quality of the modeling using its Ramachandran plot (Figure S1 of Supporting Information). This revealed that 93% of the residues were within the conventional limits. The superimposition of the ECE-2 model with the crystal structure of NEP shows that the common fold of both enzymes is composed of two largely α-helical domains. These domains form a central cavity, which contains the active site of the enzyme (Figure 2A).

Next we took advantage of the fact that both NEP and ECE-2 are inhibited by a common ligand, phosporamidon, and that the crystal structure of NEP was solved with phosphoramidon docked in its active site. We used the homology model to get information on the nature of inhibitor binding to ECE-2. For this we docked phosphoramidon into the active site of the enzyme using AutoDock (version 3/0/5) (Figure 2A, inset).

The results from the superimposition of the active site residues of NEP and ECE-2 (with the inhibitor docked) demonstrate that most of the residues are structurally aligned, including the zinc binding residues H602, H606, and E662, the catalytic E603 of the HExxH motif and the ExxxD consensus sequence. Interestingly, a third consensus sequence that is conserved among the NEP family members, N−A−Ar−Ar (where Ar indicates

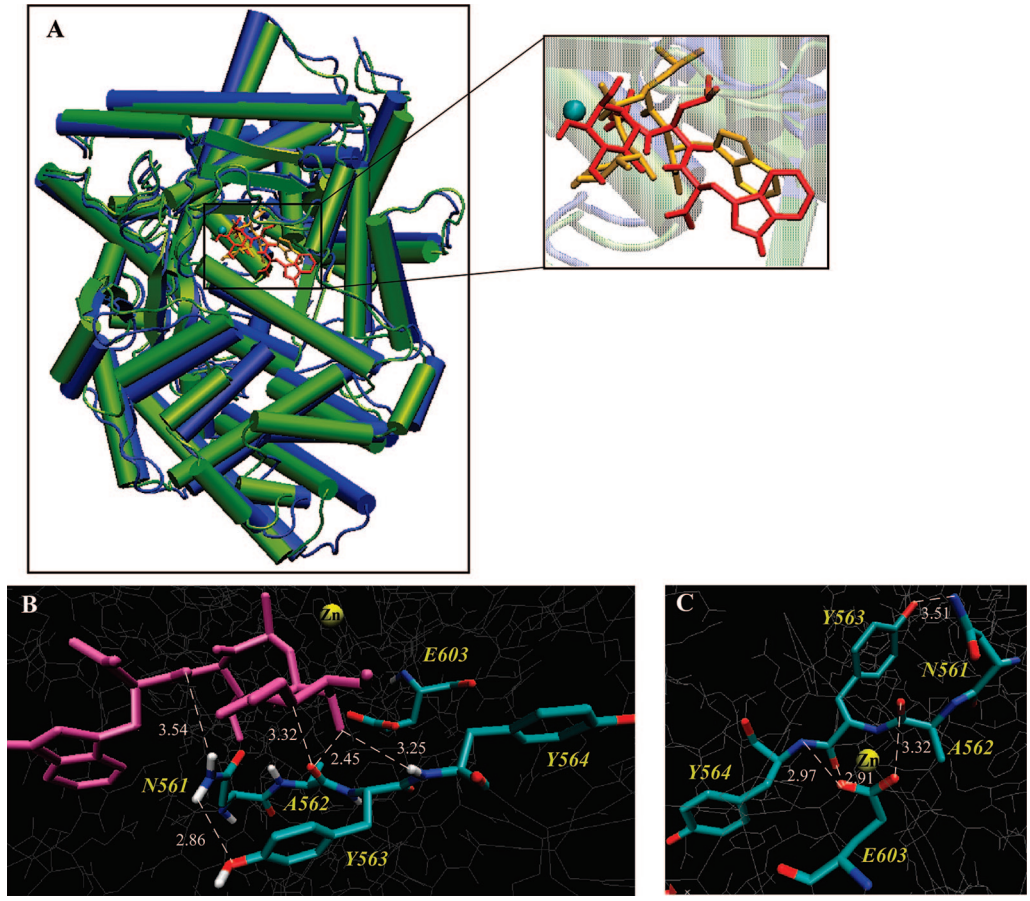

Figure 2. Comparison of the ECE-2 model with the NEP crystal structure. (A) Superimposition of diagrams of the X-ray structure of NEP (blue) and the model of ECE-2 (lime) reveals structural similarity of these two proteins. Cylinders represent α-helices. The inset depicts the position of phosphoramidon in the active site of NEP (yellow) and ECE-2 (red). The position of phosphoramidon in the ECE-2 model was calculated using Autodock (version 3/0/5). The Zn^{2+} ion is shown as a cyan sphere. (B) 3D representation of ECE-2 active site with docked phosphoramidon (purple) highlighting the binding of the inhibitor to the residues of the ^{561}NAYY^{564} consensus sequence. (C) 3D representation of the active site of ECE-2 highlighting the residues of the ^{561}NAYY^{564} consensus sequence that contribute to the positioning of the catalytic Glu 603. The images B and C were generated using VMD software.

aromatic residues), exhibits differences in structural alignment. This sequence in NEP consists of ^{542}NAFY^{545}, whereas in ECE-2 it consists of ^{561}NAYY^{564}. From the crystal structure of NEP it is clear that A543 is hydrogen-bound with the peptide amide group of the P1′ residue of phosphoramidon and N542 forms two hydrogen bonds with the NH and CO groups of the P2′ residue of the inhibitor.[11] Our analysis of the active site of ECE-2 reveals that both the N561 and A562 form hydrogen bonds with the inhibitor in a manner similar to that in NEP.[11] However, the presence of Y563 (compared to F544 in NEP) leads to changes in binding properties such as the binding orientation and interaction with phosphoramidon (Figure 2B). In addition, our model indicates that this Y563 participates in a network of hydrogen bonds with several residues including the catalytic E603. Therefore, Y563 could contribute to the positioning and orientation of E603 and thus is likely to be important for the catalytic activity/inhibitor binding of ECE-2 (Figure 2C).

An additional difference revealed from the comparison of NEP and ECE-2 is in the S2′ pocket of the binding site: R110 in NEP is replaced with W148 in ECE-2. The side chains of R102, D107, and R110 form the S2′ pocket and provide the space to hold the indole moiety of phosphoramidon. We therefore predicted that the presence of Y563 in the position of F544 and of W148 in the position of R110 could lead to changes in the binding of the inhibitor and the substrate, since previous studies have shown that phosphoramidon binds to NEP in the substrate binding pocket.

Construction and Expression of Recombinant ECE-2s. In order to test these predictions and to investigate the functional roles of Y563 and W148 residues, we performed site-directed mutagenesis. These residues present in the active site of ECE-2 were replaced with the corresponding residues from the NEP sequence: W148R and Y563F. ECE-2 and the mutated enzymes were expressed as soluble secreted proteins in an eukaryotic expression system as described previously.[18] To examine if the mutations affected the expression and secretion of proteins, we carried out Western blotting analysis with a polyclonal antiserum generated against the C-terminal of ECE-2 (Figure 3A). A band of equal intensity at ~85 kDa (corresponding to ECE-2 lacking transmembrane and N-terminal domains) was detected in all cases, thus confirming that the mutations did not affect protein expression levels. Next we subjected the medium containing the recombinant proteins to purification by anion exchange and metal ion affinity chromatography. The ECE-2 activity was measured using the quenched fluorescent peptide substrate McaBk2.[18,29] The purification efficiency of ECE-2 activity is presented in Table S1. The purified proteins were assessed for enzyme activity and intensity (by Western blot using anti-ECE-2 antibody, Figure 3B). Similar to wild type ECE-2, purified mutant enzymes were able to hydrolyze McaBk2 and the maximal activity was observed at pH 5.5.

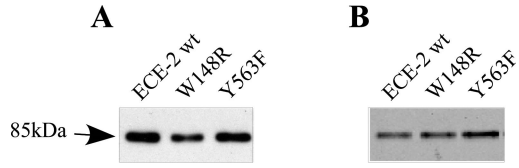

Figure 3. Expression and purification of wild type and mutated ECE-2s. (A) Western blot analysis of medium infected with baculovirus expressing wild type and mutated ECE-2s. The ECE-2 recombinant protein was detected with anti-ECE2 antiserum raised against the C-terminal region of the protein. (B) Western blot analysis of purified proteins. Recombinant protein containing medium was subjected to purification by ion exchange and metal ion chromatography, and equal amounts of the resultant fractions were run on SDS−PAGE. Protein was visualized using the anti-ECE-2 antiserum.

Determining the Kinetic Parameters of Recombinant ECE-2s. The enzymatic activity of purified wild type and mutated ECE-2s was analyzed by determining the kinetic parameters (K_m and k_{cat}) at pH 5.5 using McaBk2 as a substrate. As shown previously, this substrate is readily hydrolyzed by ECE-2 with a K_m of 5.76 ± 0.55 μM and k_{cat} of 8.51 ± 1.3 min^{-1} ($n = 3$). The mutant W148R (substitution of Trp 148 to Arg in the S2′ pocket of ECE-2) exhibits a slight but significantly increased substrate binding to the enzyme; however, this did not have an effect on the rate of hydrolysis, resulting in a k_{cat}/K_m ratio comparable to that for the wild type enzyme (Figure 4A and Table 1). In contrast, the mutant Y563F (with the substitution of Tyr 563 to Phe) exhibited no significant alterations in the K_m value but showed a significant decrease in the rate of hydrolysis, thus resulting in more than 5-fold decrease in k_{cat}/K_m ratio (Figure 4A and Table 1) indicating the importance of this residue for the catalytic activity of ECE-2.

Potency of Phosphoramidon To Inhibit Recombinant ECE-2s. Next we examined the extent to which the substitutions (W148R and Y563F) affected inhibitor binding. For this the potency of phosphoramidon, the generic metalloprotease inhibitor, to inhibit the activity of wild type and mutated ECE-2s was examined. As shown previously, phosphoramidon is a potent inhibitor of ECE-2 activity[12] and inhibits the wild type enzyme with a K_i of 1.56 ± 0.23 nM ($n = 4$) (Table 1). We find that the Y563F mutation results in a significant decrease in inhibition compared to the wild type enzyme (Figure 4B and Table 1). In contrast, the W148R mutation had no significant effect on the inhibitor potency (Table 1). We also tested the sensitivity of mutated enzymes to thiorphan, a specific inhibitor of NEP, which has previously been shown to not inhibit ECE-2 activity.[12] Consistent with this, we find that a high concentration of thiorphan (10 μM) had no significant effect on the activity of wild type or the mutated ECE-2s (data not shown). Taken together these results show that mutating Y563 affects inhibitor binding and catalysis, in agreement with our prediction. Thus, by verification of our 3D molecular model of ECE-2, these results suggest that the model could be used to screen for selective inhibitors of ECE-2.

Inhibitor Screening. To identify specific inhibitors of ECE-2, we screened a library of about 13 000 small, druglike compounds from a chemical library obtained from ChemBridge. This library was generated by combining three individual libraries: CNS-Set, DIVERSet, and MicroFormats. The combined library represents a collection of a diverse set of compounds carefully selected to provide the broadest pharmacophore coverage (and display more than 260 000 unique three-point pharmacophores). First, we subjected the library of molecules to virtual docking onto the 3D model of ECE-2 using the AutoDock program. The compound library was screened by docking the target to the known binding site inside the large cavity of the ECE-2 model. To obtain inhibitors that are specific to ECE-2, we used a two-pronged approach. First, with the help of the Dockres program, we selected top-scoring ligands that dock closest to residues in the binding site specific to ECE-2. Second, we screened the same library by docking to the crystal structure of NEP (without the ligand and crystallographic water but with Zn^{2+}). Those ligands that scored high in docking to both proteins were disregarded. The top-scoring 40 compounds that displayed the highest binding energy (> -13 kcal/mol^{-1} on the estimated free energy scale) to ECE-2 were selected. We then tested if these compounds could inhibit the activity of ECE-2 in vitro. The screening showed that at 10 μM concentration two compounds, 5719593 (**1**) and 5871159 (**2**), were able to reduce ECE-2 activity by more than 70% (Figure 5A). When these compounds were further characterized using dose-dependent inhibition curves, we found that they displayed IC_{50} values in the low ($\sim$6 μM) micromolar range (Figure 5B,C). To test the selectivity of these compounds, we measured their inhibitory potency on NEP activity and found that they exhibited $\sim$10 fold lower potency toward NEP compared to ECE-2 (Figure 5C). To further investigate the nature of this inhibition (competitive vs noncompetitive) of ECE-2 activity by these inhibitors, we determined the rate of McaBk2 hydrolysis by ECE-2 in the presence of increasing concentrations of the substrate. Analysis of the data using Lineweaver−Burk plots revealed that both compounds **1** and **2** display mixed inhibition (i.e., exhibit features of both competitive and noncompetitive inhibitors) (Figure S2). At lower concentrations they exhibit competitive inhibition and increase K_m. This is expected because they were selected to bind to the substrate-binding pocket of the ECE-2 model. However, at higher concentrations these compounds display mixed, competitive and noncompetitive, inhibition because they also decrease the V_{max} of the hydrolysis. This is likely due to the binding of the inhibitors to additional sites (other than the active site). Alternatively, at higher concentrations the binding of the inhibitors could alter the conformation of the active site such that it could affect substrate binding. Both of these scenarios would lead to a noncompetitive type of inhibition.

In order to probe the structures of these two compounds and define parameters important for inhibitor binding, we searched the ZINC database of commercially available compounds for analogues of the two selected compounds.[30] Thirty compounds from the database were docked to the active site of our 3D molecular model of ECE-2 using AutoDock software as described earlier. Three analogues of **1** that exhibited highest binding affinity, **3** (S136492), **4** (6634449), and **5** (6636797), were selected for biochemical analysis. Examination of their inhibitory potency revealed **3** to be the most potent (with a low micromolar potency similar to that of **1**). Interestingly the other two compounds exhibited 5 times reduced potency, suggesting that the additional CH_3 group in the P1′ position plays an important role in the binding and inhibition (Figure 6).

Thus, using a combination of homology modeling and virtual screening, we have been able to identify selective inhibitors of ECE-2. Docking of the inhibitors to the active site of ECE-2 in the molecular model reveals that these compounds bind in the vicinity of Zn^{2+} atom and form multiple interactions with the

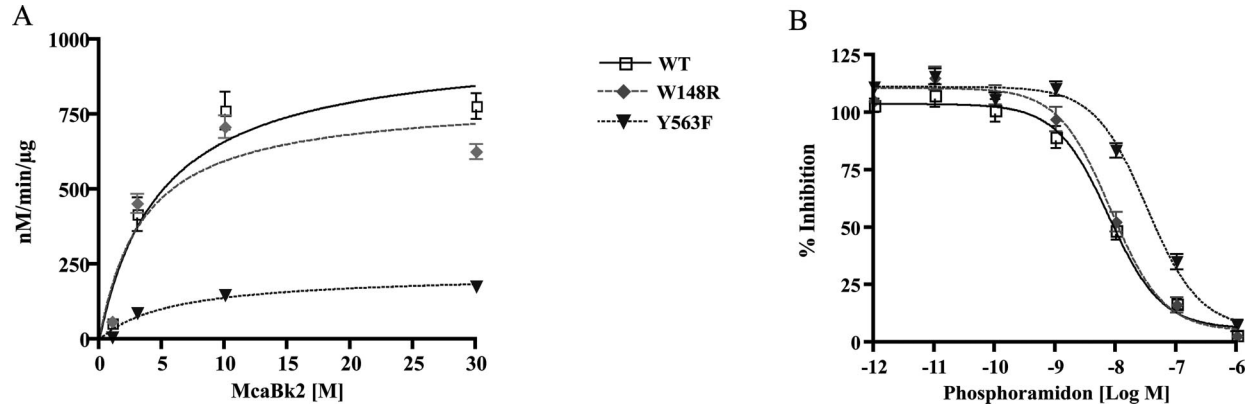

Figure 4. Initial rate of substrate hydrolysis and inhibition by phosphoramidon of wild type (WT) and mutated ECE-2s. (A) The initial rate of substrate hydrolysis (V_0) at final concentrations of 0.1−30 μM was determined by measuring the appearance of product under initial rate conditions. V_0 values were plotted as a function of substrate concentration ([S]) and fit to the Michaelis−Menten equation. Data represent the mean ± SEM ($n = 3$). (B) Dose-dependent inhibition curve for phosphoramidon was generated by measuring the substrate hydrolysis in the presence of inhibitor at concentrations of 1 nM to 1 μM. Data represent the mean ± SEM ($n = 4$).

Table 1. Kinetic Parameters and Inhibition of Wild Type and Mutated ECE-2s by Phosphoramidon[a]

enzymes	K_m (mM)	k_{cat} (min^{-1})	k_{cat}/K_m (mM^{-1} min^{-1})	K_i (nM)
ECE-2 WT	5.76 ± 0.55	8.51 ± 1.32	1.48 ± 0.23	1.56 ± 0.23
W148R	3.94 ± 0.15*	6.84 ± 0.57	1.74 ± 0.15	1.58 ± 0.21
Y563F	6.60 ± 1.37	2.10 ± 0.11**	0.32 ± 0.02**	11.07 ± 2.36***

[a] The kinetic parameters (K_m and k_{cat}) of the purified enzymes were determined from Michaelis−Menten plots. Inhibition of recombinant enzymes by phosphoramidon (K_i) was determined from dose-dependent inhibition curves for a final McaBk2 concentration of 10 μM. Data represent the mean ± SEM ($n = 3$): (*) $p < 0.05$; (**) $p < 0.005$; (***) $p < 0.001$.

residues of the active site involved in substrate binding and catalysis (Figure 7).

Discussion

ECE-2 is a recently identified member of M13 family of zinc metallopeptidases of which NEP is the best characterized. Until recently most of the structural information about these enzymes was based on the studies carried out on the bacterial homologue thermolysin (TLN). Although there is very limited homology between the primary sequences of TLN and NEP, these two enzymes have similar catalytic properties and are inhibited by the same type of molecules such as phosphoramidon and thiorphan. In addition, they both contain the highly conserved consensus sequences, HExxH and ExxxD, which contain residues critical for Zn^{2+} coordination and catalysis. On the basis of early crystallographic studies, Matthews proposed a mechanism for the TLN-catalyzed cleavage of peptides.[31] According to this model, the two His residues (H142 and H146) together with the E166 and a water molecule are involved in the tetrahedral coordination of the Zn^{2+} atom. The incoming substrate displaces the water molecule toward the catalytic E143 residue. The negative charge of E143 polarizes the zinc-coordinated water molecule and promotes its nucleophilic attack on the carbonyl carbon of the scissile peptide bond. Structural studies also indicated the importance of H231 and Y157 residues in the stabilization of the transition state.

Later studies in NEP using site-directed mutagenesis have identified corresponding residues involved in zinc coordination, catalysis, and substrate binding and confirmed that the proposed catalytic mechanism was also valid for the mammalian enzymes.[19–26] Several studies also modeled the structure of NEP, as well as other family members using the crystal structure of TLN as a template. However, the availability of the crystal structure of NEP complexed with phosphoramidon provides a more suitable and reliable template for the modeling of metallopeptidases of this family and has therefore been used to model the structures of several members of M13 family, including endothelin-converting enzyme-1 (ECE-1), Kell blood group protein, and neprilysin-2 (NEP-2).[32–34] ECE-1 and ECE-2 share common substrates and approximately 60% sequence homology. The consensus sequences that are conserved among zinc metallopeptidases are identical between these two proteins, indicating significant structural similarities. Therefore, the molecular model of ECE-1 could provide considerable information about the architecture of the ECE-2 active site.[32] However, since the molecular model of ECE-1 was not deposited in the PDB, a detailed comparison of our model with that of ECE-1 was not possible.

There are a number of important physiological differences between ECE-1 and ECE-2, such as the pH dependency and sensitivity to inhibition by phosphoramidon.[12] This generic metallopeptidase inhibitor is ~100 less potent toward ECE-1 ($IC_{50} = 3.5$ μM) than ECE-2 and NEP ($IC_{50} = 2-4$ nM), suggesting that despite a number of similarities, some aspects of catalysis and inhibitor binding to the active site of each of these peptidases could be quite distinct. In addition, the detailed information about the binding pocket of each of these peptidases will be useful to design specific and selective inhibitors of ECE-1 and ECE-2. Because of the involvement of ET in various cardiovascular, renal, pulmonary, and central nervous system diseases,[35–37] much effort has been put toward developing inhibitors of this pathway as potential therapeutic agents. In this light, inhibitors of ECE, which catalyze a rate-limiting step in ET production, have received a great deal of attention. In addition, double inhibitors of ECE and NEP that would interfere with the production of ET, a vasoconstrictor, as well as with the degradation of atrial natriuretic peptide (ANP), a potent vasorelaxant, have also been designed as potential therapeutics for the treatment of hypertension.[38] However, most of these studies did not differentiate between ECE-1 and ECE-2 and focused on the inhibition of ECE-1 activity without addressing the effect of these inhibitors on ECE-2. To date, only a trisubstituted quinazoline, PD069185 (**6**) (Chart 1), and its analogues have been tested and reported to be selective for ECE-1 over ECE-2.[39]

In order to help us identify specific inhibitors of ECE-2, we generated a 3D molecular model of ECE-2 based on the X-ray structure of NEP. A comparison of the active sites of these two

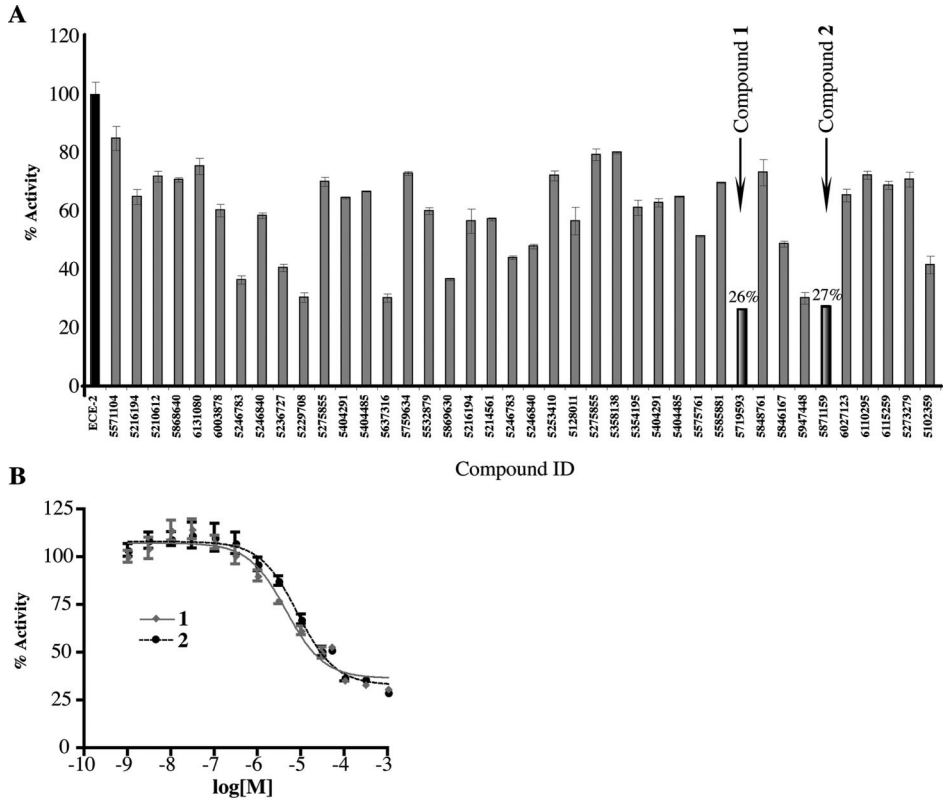

Figure 5. Screening of compounds for the inhibition of ECE-2 activity. (A) The rate of McaBk2 fluorescent substrate hydrolysis by recombinant ECE-2 was measured in the absence and presence of 10 μM of each of 40 top scoring compounds by initial screening. Data are represented as percent activity of ECE-2 without inhibitor. The two most potent compounds, **1** and **2**, inhibited ECE-2 activity by more than 70%. (B) Concentration-dependent inhibition curves for selected inhibitor compounds, **1** and **2**, were generated by measuring substrate hydrolysis in the presence of inhibitors at concentrations of 1nM to 1 mM. (C) IC_{50} values for each selected inhibitor compound were determined for ECE-2 and NEP by establishing concentration-dependent inhibition curves for a final McaBk2 concentration of 10 μM. Data represent the mean ± SEM ($n = 5$).

enzymes revealed that the residues involved in catalysis as well as the residues in the vicinity of the substrate/inhibitor binding pocket that interact with the substrate are highly conserved. However, we identified two amino acid differences in the active sites of NEP and ECE-2, which could potentially account for pharmacological differences between NEP and ECE-2.

One of the residues, F544 of NEP within the conserved consensus sequence ^{542}NAFY^{545}, is substituted by Y563 in ECE-2 and Y552 in ECE-1. On the basis of earlier mutagenesis studies as well as crystal structure, both N542 and A543 of NEP were shown to form hydrogen bonds with phosphoramidon.[11,25] Sansom and colleagues[40] also demonstrated the importance of Y552 within this sequence, for the catalytic activity of ECE-1. Although in the ECE-2 model Y563 was not found to directly interact with the phosphoramidon, it was found to hydrogen-bond to N561 and thus affect inhibitor binding. Y563 is also in a position to interact with the catalytic E603. While the distance between these two residues suggests only a weak interaction, even a slight movement of the catalytic Glu could have a drastic effect on the catalytic activity of the enzyme. Indeed, we found that the substitution of the Tyr 563 residue with Phe in ECE-2 resulted in approximately 6-fold lower catalytic activity for the enzyme and more than 7-fold decrease in inhibitor potency. The fact that this mutation did not influence substrate binding but affected inhibition by the transition state analogue phosphoramidon leads us to hypothesize that Y563 may be involved in the catalytic activity and in the stabilization of the transition state of the enzyme, by participating in the positioning and orientation of E603. Considering that this substitution is very conservative, such small, albeit significant change in enzyme properties demonstrates the importance of this residue for the catalytic activity of ECE-2.

Another difference we found in the active site of these two enzymes is that the Arg 110 residue in NEP is substituted by

A

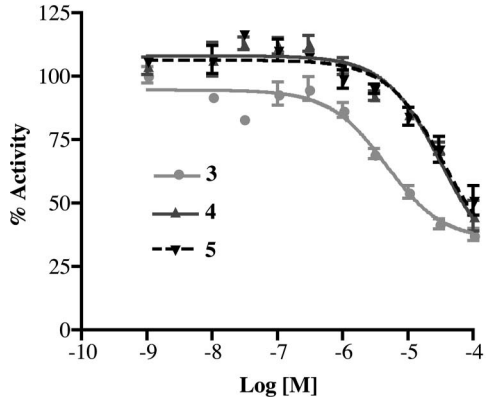

B

Inhibitor	IC50 (μM)	Structure
Compound **3**	4.63	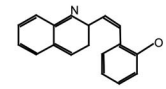
Compound **4**	32.9	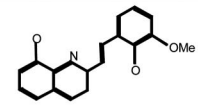
Compound **5**	35.7	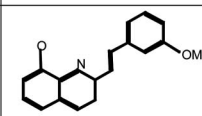

Figure 6. Inhibition of ECE-2 activity by **1** analogues. (A) Concentration-dependent inhibition curves for three selected analogues, **3**−**5**, were generated by measuring the substrate hydrolysis in the presence of inhibitors at concentrations of 1 nM to 100 μM. (B) IC_{50} values for each selected inhibitor compound were determined by establishing concentration-dependent inhibition curves for a final McaBk2 concentration of 10 μM. Data represent the mean ± SEM ($n = 4$).

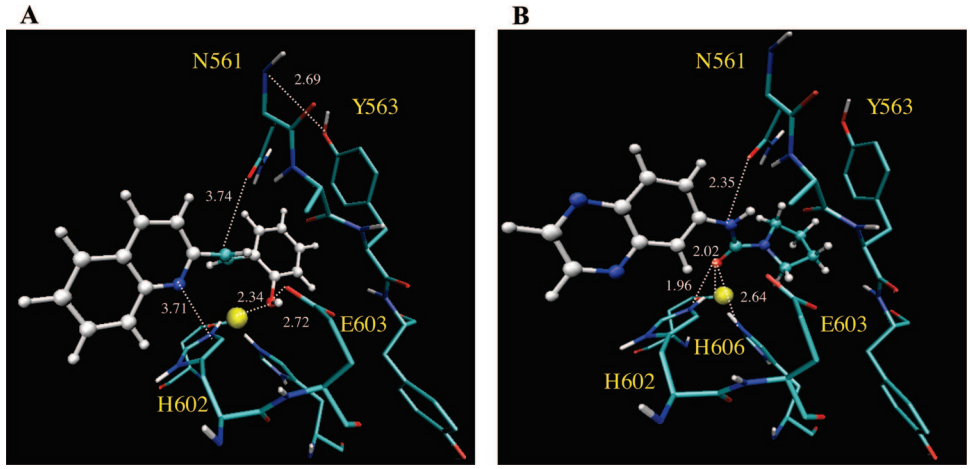

Figure 7. Binding of inhibitor compounds to the molecular model of the active site of ECE-2. The images highlight the binding of **1** (A) and **2** (B) to the H602 and H606 involved in zinc coordination, catalytic E603 and residues of the ^{541}NAYY^{544} consensus sequence. The images were generated using VMD software.

Chart 1. Structure of Compound **6**[39]

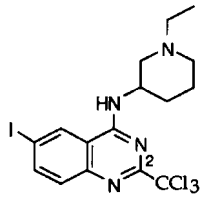

Trp in ECE-2. R110 is one of the residues that along with R102 and D107 form the S2′ subsite of NEP. In ECE-2 this subsite is large, similar to NEP, and can accommodate bulky side chains. The presence of Trp in place of R110 could result in a wider pocket with reduced specificity. We observed that mutation of Trp 148 back to Arg slightly but significantly increased affinity for the substrate; however, it did not affect the inhibitor potency. The change in affinity may be explained by the fact that the McaBk2 peptide has a Lys residue in the P2′ position, and its long side chain is held tighter in the S2′ pocket with the reduced volume. The more compact Trp side chain of the inhibitor phosphoramidon in the S2′ pocket is not affected by this change. Testing additional substrates with different residues in P2′ position is needed to address this notion.

After confirming the validity of the 3D molecular model of ECE-2 by site-directed mutagenesis, we used the model to screen a library of approximately 13 000 small druglike molecules. Initially the structures of the compounds were docked into the active site of the ECE-2 model. Compounds that displayed the highest binding were tested experimentally using an in vitro enzyme assay. In the experimental screening we identified two compounds, **1**and **2**, that inhibited ECE-2 activity with micromolar potency and were ∼10 times more selective for ECE-2 compared to NEP. We found that these compounds also inhibit ECE-1 activity with an affinity similar to that of ECE-2 (Gagnidze and Devi, unpublished results). This is not surprising because the homology between ECE-2 and ECE-1 is higher than that between ECE-2 and NEP and because Y563 of ECE-2 is also conserved in ECE-1. Furthermore, Y563 in ECE-1 has been shown to play a role in the catalytic activity of the enzyme.[40]

An examination of the docking of these compounds to the active site of ECE-2 revealed that they bind in proximity to the Zn^{2+} atom and are in a position to form hydrogen bonds with the His residues that coordinate Zn^{2+} as well as the catalytic Glu 603. Thus, they are in a position to affect the hydrolysis of the substrate (Figure 7). In order to identify compounds with higher inhibitory potency toward ECE-2, we searched for

analogues of **1** and found three compounds that were commercially available. Two of these three analogues, **4** and **5**, were ~5−6 times less effective compared to **1**. These two compounds have additional CH_3 groups in the P1′ position, and this may interfere with the stringent specificity of S1′ site that is characteristic of these metallopeptidases. An optimal way to increase the potency of these inhibitors would be through chemical optimization using the structures of **1** and **2** as a lead. Additional analyses are also needed to ensure the selectivity of these compounds for ECE-2, and the chemical optimization may be a useful strategy to achieve this goal as well. Information from these studies will be useful in the identification of specific inhibitors of ECE-2 that will serve as hitherto unavailable tools for studies examining the physiological role of this peptidase in vivo.

Conclusions

Endothelin-converting enzyme-2 belongs to the M13 family of Zn^{2+} metallopeptidases and shares a substantial structural similarity with its homologue neprilysin. We used the crystal structure of NEP to generate a 3D molecular model of ECE-2. Analyses of the architecture of the active site and the binding specificities of the inhibitor phosphoramidon to the enzyme led us to identify two nonconserved residues that affect the catalytic activity and substrate/inhibitor binding of ECE-2. Tyr 563 of ECE-2 is part of the conserved consensus sequence ^{561}NAYY^{564} and participates in a network of hydrogen bonds with the catalytic Glu 603. Mutation of Tyr 563 of ECE-2 to Phe results in more than 4-fold decrease of k_{cat} of the peptidase. Tyr 563 is also involved in the binding and positioning of the inhibitor phosphoramidon in the active site of ECE-2, and the substitution of this residue with Phe attenuates the inhibition by phosphoramidon by almost 10-fold. The second nonconserved residue Trp 148 is located in the S2′ site of the catalytic cleft of ECE-2 that harbors the indole moiety of phosphoramidon. Substitution of this residue to Arg affected substrate binding without influencing catalytic activity of the enzyme or binding of the inhibitor.

The 3D molecular model of ECE-2 was next used to screen inhibitor compounds for their binding to the active site of the enzyme, and a number of selected compounds were tested experimentally. The tests led to the identification of three compounds, **1**−**3**, that inhibited ECE-2 activity with IC_{50} values in the lower micromolar range and displayed higher selectivity toward ECE-2 versus NEP. These compounds can be used in future studies as leads for the development of potent and specific inhibitors of ECE-2 and will aid in the elucidation of the physiological functions of the peptidase.

Experimental Section

Homology Modeling. The model building of ECE-2 using NEP structure (PDB code 1DMT) was achieved using MODELER 8v2 program.[41,42] The quality of the model was checked using PROCHECK[43,44] and ProSa 2003.[45,46] A Ramachandran plot generated in PROCHECK with a hypothetical resolution of 3.0 Å revealed that 93% of the amino acid residues are in the most favorable region. The alignment of two the protein structures was carried out using the "align" command of pymol, which works by doing a sequence alignment and then trying to align the structures to minimize the rmsd between the aligned residues. A rmsd value of 0.36 Å was obtained between ECE-2 and NEP by aligning all atoms against the entire C-α backbone. The *Z*-score, calculated using the software ProSa 2003, showed that the predicted model of ECE-2 was well within the range of a typical native structure.

Molecular Docking. Docking of phosphoramidon to NEP and ECE-2 was achieved using AutoDock, version 3.0.5,[47,48] which uses a genetic algorithm as a global optimizer combined with energy minimization as a local search method. The starting structure of phosphoramidon was taken from the X-ray structure (PDB code 1DMT), and the partial charges were assigned using Gasteiger−Marsili method using AutoDockTools (http://mgltools.scripps.edu/downloads). Autotors program was used to define torsional degrees of freedom in the ligand, and a total of eight torsions were allowed. Binding-site-centered affinity grid maps were generated for NEP with 0.375 Å spacing using Autogrid for NEP. The minimization was achieved using Lamarckian genetic algorithm (LGA) and pseudo Solis and Wets method.[49] The grid size was set to 50 × 50 × 60 points, centered on the Zn^{2+} atom in the crystal structure of the complex. Each LGA job consisted of 200 runs with 270 000 generations in each run, and the maximum number of energy evaluations was set to 5.0×10^6. Resulting docked conformations within 1.0 Å rmsd tolerance of each other were clustered together and analyzed using AutoDockTools. The zinc parameters used were the following: radius $r = 1.1$ Å, well depth $\varepsilon = 0.35$ kcal/mol, and a charge of +1.0 e.

Inhibitor Screening. For the inhibitor screening we used a chemical library from ChemBridge that was generated by combining three individual libraries from CNS-Set, DIVERSet, and MicroFormats. The combined library represents a collection of a diverse set of druglike, small molecule compounds carefully selected to provide the broadest pharmacophore coverage (and display more than 260 000 unique three-point pharmacophores). For virtual screening, the AutoDock program (version 3.05) was used. The screening was driven by scripts for our cluster of Apple G5 processors running in parallel, and the analysis and filtering were done by the program Dockres (URL: http://inka.mssm.edu/~mezei/dockres),

Materials. Internally quenched fluorescent substrate McaBk2 ((7-methoxycoumarin-4-yl)acetyl-RPPGFSAFL-(2,4-dinitrophenyl)) was custom-synthesized by Open Biosystems (Huntsville, AL). DEAE-Sepharose fast flow was obtained from Amersham Biosciences AB (Uppsala, Sweden), and Talon metal affinity resin was purchased from Clontech (Palo Alto, CA). Inhibitor compounds were purchased from ChemBridge Corporation (San Diego, CA) and are identified by database ID. Compound **3** was purchased from Sigma-Aldrich's Rare Chemical Library (St. Louis, MO).

Cloning and Site-Directed Mutagenesis. The cloning of a secreted soluble form of ECE-2 was described previously.[18] The same construct was used as a template to introduce the two mutations: W148R and Y563F. Two overlapping regions of the ECE-2 sequence were amplified separately using two flanking oligonucleotides, Forw-5′-TCATCATGCCCTAGGGGTC-3′ and Rev-5′-CTGCAGCGGCCGCGACCTG-3′, in combination with two overlapping oligonucleotides containing the mutated residues: (W148R) 5′-CAGCCTCAGGGACCAAAAC 3′ and (Y563F) 5′ACAGTGAATGCCTTCTACCTTCCAACT 3′.

The products of the first round of amplification were used as the template for a second PCR with the two flanking oligonucleotides. The final PCR product was digested and cloned into the baculovirus expression vector pVL1393. The DNA constructs were sequenced to ensure that correct mutations were introduced. The recombinant virus production was carried out as described previously.[18]

Expression and Purification of Soluble ECE-2s. Sf9 insect cells growing in Baculo Gold Max-XP serum-free insect cell medium (BD Biosciences, San Jose, CA) were co-transfected with recombinant wild type and mutated ECE-2 cDNA in pVL1393 and BaculoGold viral DNA (BD Biosciences) using the calcium phosphate procedure. After culturing for 5 days, amounts of 100−500 μL of medium were used to infect 3×10^5 Sf9 cells in a 25 cm^2 flask. Then 1 mL of the medium containing amplified virus was used to infect 3×10^5 Sf9 cells in 5 mL of medium in 25 cm^2 flasks. After 3 days of infection, the medium was collected and cleared by centrifugation at 20000*g* for 10 min, and the resulting supernatant was frozen at −80 °C until use. Wild type and mutated ECE-2-containing conditioned media were concentrated using Amicon ultrafiltration membrane YM100 (Millipore Corp., Bedford, MA), and purified using DEAE-Sepharose anion exchange column

and Talon-Sepharose Co^{2+} affinity resin column as described in Supporting Information. Fractions containing ECE-2 activity were subjected to SDS−PAGE and visualized by Western blot. The amounts of purified recombinant mutant ECE-2 proteins used in all subsequent experiments were normalized to that of wild type ECE-2.

Western Blotting. The expression of wild type and mutated ECE-2s in the conditioned media from the baculovirus infected Sf9 cells was analyzed by Western blotting. An amount of 25 μg of total protein was separated by sodium dodecyl sulfate polyacrylamide gel electrophoresis, transferred onto a nitrocellulose membrane, and blotted with a polyclonal antiserum generated against the C-terminal 16 amino acids of ECE-2 (1:1000). This antiserum has been previously characterized and is able to recognize the ~85 kDa truncated form of ECE-2 secreted from baculovirus cells.[18] There was no significant difference in the expression levels of wild type and mutated ECE-2 recombinant proteins.

Assay for ECE-2 Activity. Enzyme activity was assayed using the synthetic quenched fluorescent substrate McaBk2. The assay was carried out at 37 °C with 10 μM McaBk2 in 0.2 M sodium acetate buffer, pH 5.5, containing the detergent $C_{12}E_8$ (octaethylene glycol dodecyl ether, EMD Chemicals, Inc., San Diego, CA) unless otherwise indicated. Substrate hydrolysis was monitored on a Fluoromax plate reader with excitation at 335 nm and emission at 440 nm, and initial velocity was determined.

Determination of Kinetic Constants for ECE-2. The enzymatic parameters of the wild type and mutated ECE-2s were determined in a microtiter plate by monitoring the rate of hydrolysis of a synthetic substrate, McaBk2, in sodium acetate buffer, pH 5.5, at 37 °C. The initial rate of substrate hydrolysis (V_0) at final concentrations of 0.1−30 mM was determined by measuring the appearance of product under initial rate conditions. V_0 values were plotted as a function of substrate concentration ([S]) and fit to the Michaelis−Menten equation using GraphPad Prism software (version 4.0b). The sensitivity of wild type and mutated ECE-2s to inhibition by phosphoramidon and inhibitor compounds was determined by establishing dose-dependent inhibition curves, and data analysis was done using GraphPad Prism software (version 4.0b).

Acknowledgment. We thank Dr. Sherwin Wilk for the help with some of the studies and Dr. Ivone Gomes for reading the manuscript. These studies are supported by NIH (Grants NS26880 and DA019521 to L.A.D. and Grant CA87658 to M.-M.Z.).

Supporting Information Available: Ramachandran plot of ECE-2 model, characterization of inhibition, and table of purification of ECE-2 activity. This material is available free of charge via the Internet at http://pubs.acs.org.

References

(1) Docherty, K.; Steiner, D. F. Post-translational proteolysis in polypeptide hormone biosynthesis. *Annu. Rev. Physiol.* **1982**, *44*, 625–638.

(2) Steiner, D. F. The proprotein convertases. *Curr. Opin. Chem. Biol.* **1998**, *2* (1), 31–39.

(3) Mizuno, K.; Minamino, N.; Kangawa, K.; Matsuo, H. A new family of endogenous "big" Met-enkephalins from bovine adrenal medulla: purification and structure of docosa- (BAM-22P) and eicosapeptide (BAM-20P) with very potent opiate activity. *Biochem. Biophys. Res. Commun.* **1980**, *97* (4), 1283–1290.

(4) Yang, H. Y.; Fratta, W.; Majane, E. A.; Costa, E. Isolation, sequencing, synthesis, and pharmacological characterization of two brain neuropeptides that modulate the action of morphine. *Proc. Natl. Acad. Sci. U.S.A.* **1985**, *82* (22), 7757–7761.

(5) Sigafoos, J.; Chestnut, W. G.; Merrill, B. M.; Taylor, L. C.; Diliberto, E. J., Jr.; Viveros, O. H. Novel peptides from adrenomedullary chromaffin vesicles. *J. Anat.* **1993**, *183* (Part 2), 253–264.

(6) Che, F. Y.; Yan, L.; Li, H.; Mzhavia, N.; Devi, L. A.; Fricker, L. D. Identification of peptides from brain and pituitary of Cpe(fat)/Cpe(fat) mice. *Proc. Natl. Acad. Sci. U.S.A.* **2001**, *98* (17), 9971–9976.

(7) Perry, S. J.; Yi-Kung Huang, E.; Cronk, D.; Bagust, J.; Sharma, R.; Walker, R. J.; Wilson, S.; Burke, J. F. A human gene encoding morphine modulating peptides related to NPFF and FMRFamide. *FEBS Lett.* **1997**, *409* (3), 426–430.

(8) Vilim, F. S.; Aarnisalo, A. A.; Nieminen, M. L.; Lintunen, M.; Karlstedt, K.; Kontinen, V. K.; Kalso, E.; States, B.; Panula, P.; Ziff, E. Gene for pain modulatory neuropeptide NPFF: induction in spinal cord by noxious stimuli. *Mol. Pharmacol.* **1999**, *55* (5), 804–811.

(9) Ahn, K. In *Handbook of Proteolytic Enzymes*; Academic Press: San Diego, CA, 1998; pp 1085−1089.

(10) Molineaux, C.; Wilk, S. *Extracellular Processing of Peptides*; CRC Press: Boca Raton, FL, 1991; Chapter 10, pp 251−282.

(11) Oefner, C.; D'Arcy, A.; Hennig, M.; Winkler, F. K.; Dale, G. E. Structure of human neutral endopeptidase (Neprilysin) complexed with phosphoramidon. *J. Mol. Biol.* **2000**, *296* (2), 341–349.

(12) Emoto, N.; Yanagisawa, M. Endothelin-converting enzyme-2 is a membrane-bound, phosphoramidon-sensitive metalloprotease with acidic pH optimum. *J. Biol. Chem.* **1995**, *270* (25), 15262–15268.

(13) Turner, A. J.; Murphy, L. J. Molecular pharmacology of endothelin converting enzymes. *Biochem. Pharmacol.* **1996**, *51* (2), 91–102.

(14) Turner, A. J.; Isaac, R. E.; Coates, D. The neprilysin (NEP) family of zinc metalloendopeptidases: genomics and function. *BioEssays* **2001**, *23* (3), 261–269.

(15) Xu, D.; Emoto, N.; Giaid, A.; Slaughter, C.; Kaw, S.; deWit, D.; Yanagisawa, M. ECE-1: a membrane-bound metalloprotease that catalyzes the proteolytic activation of big endothelin-1. *Cell* **1994**, *78* (3), 473–485.

(16) Eckman, E. A.; Reed, D. K.; Eckman, C. B. Degradation of the Alzheimer's amyloid beta peptide by endothelin-converting enzyme. *J. Biol. Chem.* **2001**, *276* (27), 24540–24548.

(17) Eckman, E. A.; Watson, M.; Marlow, L.; Sambamurti, K.; Eckman, C. B. Alzheimer's disease beta-amyloid peptide is increased in mice deficient in endothelin-converting enzyme. *J. Biol. Chem.* **2003**, *278* (4), 2081–2084.

(18) Mzhavia, N.; Pan, H.; Che, F. Y.; Fricker, L. D.; Devi, L. A. Characterization of endothelin-converting enzyme-2. Implication for a role in the nonclassical processing of regulatory peptides. *J. Biol. Chem.* **2003**, *278* (17), 14704–14711.

(19) Malfroy, B.; Schwartz, J. C. Enkephalinase from rat kidney. Purification, characterization, and study of substrate specificity. *J. Biol. Chem.* **1984**, *259* (23), 14365–14370.

(20) Devault, A.; Nault, C.; Zollinger, M.; Fournie-Zaluski, M. C.; Roques, B. P.; Crine, P.; Boileau, G. Expression of neutral endopeptidase (enkephalinase) in heterologous COS-1 cells. Characterization of the recombinant enzyme and evidence for a glutamic acid residue at the active site. *J. Biol. Chem.* **1988a**, *263* (8), 4033–4040.

(21) Devault, A.; Sales, V.; Nault, C.; Beaumont, A.; Roques, B.; Crine, P.; Boileau, G. Exploration of the catalytic site of endopeptidase 24.11 by site-directed mutagenesis. Histidine residues 583 and 587 are essential for catalysis. *FEBS Lett.* **1988b**, *231* (1), 54–58.

(22) Vijayaraghavan, J.; Kim, Y. A.; Jackson, D.; Orlowski, M.; Hersh, L. B. Use of site-directed mutagenesis to identify valine-573 in the S′1 binding site of rat neutral endopeptidase 24.11 (enkephalinase). *Biochemistry* **1990**, *29* (35), 8052–8056.

(23) Beaumont, A.; Le Moual, H.; Boileau, G.; Crine, P.; Roques, B. P. Evidence that both arginine 102 and arginine 747 are involved in substrate binding to neutral endopeptidase (EC 3.4.24.11). *J. Biol. Chem.* **1991**, *266* (1), 214–220.

(24) Kim, Y. A.; Shriver, B.; Quay, T.; Hersh, L. B. Analysis of the importance of arginine 102 in neutral endopeptidase (enkephalinase) catalysis. *J. Biol. Chem.* **1992**, *267* (17), 12330–12335.

(25) Dion, N.; Le Moual, H.; Crine, P.; Boileau, G. Kinetic evidence that His-711 of neutral endopeptidase 24.11 is involved in stabilization of the transition state. *FEBS Lett.* **1993**, *318* (3), 301–304.

(26) Dion, N.; Le Moual, H.; Fournie-Zaluski, M. C.; Roques, B. P.; Crine, P.; Boileau, G. Evidence that Asn542 of neprilysin (EC 3.4.24.11) is involved in binding of the P2′ residue of substrates and inhibitors. *Biochem. J.* **1995**, *311* (Part 2), 623–627.

(27) Sansom, C. E.; Hoang, V. M.; Turner, A. J. Molecular modeling of the active site of endothelin-converting enzyme. *J Cardiovasc Pharmacol* **1995**, *26* (Suppl. 3), S75–S77.

(28) Tiraboschi, G.; Jullian, N.; Thery, V.; Antonczak, S.; Fournie-Zaluski, M. C.; Roques, B. P. A three-dimensional construction of the active site (region 507−749) of human neutral endopeptidase (EC.3.4.24.11). *Protein Eng.* **1999**, *12* (2), 141–149.

(29) Johnson, G. D.; Ahn, K. Development of an internally quenched fluorescent substrate selective for endothelin-converting enzyme-1. *Anal. Biochem.* **2000**, *286* (1), 112–118.

(30) Irwin, J. J.; Shoichet, B. K. ZINC—a free database of commercially available compounds for virtual screening. *J. Chem. Inf. Model.* **2005**, *45* (1), 177–182.

(31) Matthews, B. W. Structural bases of the action of thermolysin and related zinc peptidases. *Acc. Chem. Res.* **1988**, *21* (9), 333–340.

(32) Bur, D.; Dale, G. E.; Oefner, C. A three-dimensional model of endothelin-converting enzyme (ECE) based on the X-ray structure of neutral endopeptidase 24.11 (NEP). *Protein Eng.* **2001**, *14* (5), 337–341.

(33) Voisin, S.; Rognan, D.; Gros, C.; Ouimet, T. A three-dimensional model of the neprilysin 2 active site based on the X-ray structure of neprilysin. Identification of residues involved in substrate hydrolysis and inhibitor binding of neprilysin 2. *J. Biol. Chem.* **2004**, *279* (44), 46172–46181.

(34) Lee, S.; Debnath, A. K.; Redman, C. M. Active amino acids of the Kell blood group protein and model of the ectodomain based on the structure of neutral endopeptidase 24.11. *Blood* **2003**, *102* (8), 3028–3034.

(35) Ferro, C. J.; Webb, D. J. The clinical potential of endothelin receptor antagonists in cardiovascular medicine. *Drugs* **1996**, *51* (1), 12–27.

(36) Kohan, D. E. Endothelins in the normal and diseased kidney. *Am. J. Kidney Dis.* **1997**, *29* (1), 2–26.

(37) Humbert, M.; Simonneau, G. Drug insight: endothelin-receptor antagonists for pulmonary arterial hypertension in systemic rheumatic diseases. *Nat. Clin. Pract. Rheumatol.* **2005**, *1* (2), 93–101.

(38) Jeng, A. Y.; Mulder, P.; Kwan, A. L.; Battistini, B. Nonpeptidic endothelin-converting enzyme inhibitors and their potential therapeutic applications. *Can. J. Physiol. Pharmacol.* **2002**, *80* (5), 440–449.

(39) Ahn, K.; Sisneros, A. M.; Herman, S. B.; Pan, S. M.; Hupe, D.; Lee, C.; Nikam, S.; Cheng, X. M.; Doherty, A. M.; Schroeder, R. L.; Haleen, S. J.; Kaw, S.; Emoto, N.; Yanagisawa, M. Novel selective quinazoline inhibitors of endothelin converting enzyme-1. *Biochem. Biophys. Res. Commun.* **1998**, *243* (1), 184–190.

(40) Sansom, C. E.; Hoang, M. V.; Turner, A. J. Molecular modelling and site-directed mutagenesis of the active site of endothelin-converting enzyme. *Protein Eng.* **1998**, *11* (12), 1235–1241.

(41) Eswar, N.; Webb, B.; Marti-Renom, M. A.; Madhusudhan, M. S.; Eramian, D.; Shen, M. Y.; Pieper, U. ; Sali, A. Comparative protein structure modeling using modeller. *Curr. Protoc. Bioinf.* **2006**, Chapter 5, Unit 5.6.

(42) Sali, A.; Blundell, T. L. Comparative protein modelling by satisfaction of spatial restraints. *J. Mol. Biol.* **1993**, *234* (3), 779–815.

(43) Laskowski, R. A.; MacArthur, M. W.; Moss, D. S.; Thornton, J. M. PROCHECK: a program to check the stereochemical quality of protein structures. *J. Appl. Crystallogr.* **1993**, *26*, 283–291.

(44) Morris, A. L.; MacArthur, M. W.; Hutchinson, E. G.; Thornton, J. M. Stereochemical quality of protein structure coordinates. *Proteins* **1992**, *12* (4), 345–364.

(45) Sipple, M. J. Recognition of errors in three-dimensional structures of proteins. *Proteins: Struct., Funct., Bioinf.* **1993**, *17*, 355–362.

(46) Ginalski, K. Comparative modeling for protein structure prediction. *Curr. Opin. Struct. Biol.* **2006**, *16* (2), 172–177.

(47) Morris, G. M.; Goodsell, D. S.; Halliday, R. S.; Huey, R.; Hart, W. E.; Belew, R. K.; Olson, A. J. Automated docking using a Lamarckian genetic algorithm and an empirical binding free energy function. *J. Comput. Chem.* **1998**, *19* (14), 1639–1662.

(48) Goodsell, D. S.; Morris, G. M.; Olson, A. J. Automated docking of flexible ligands: applications of AutoDock. *J. Mol. Recognit.* **1996**, *9* (1), 1–5.

(49) Solis, F. J.; Wets, R. J. Minimization by random search techniques. *Math. Oper. Res.* **1981**, *6* (1), 19–30.

JM7015478